

Dynamic evolution of S_0 - S_3 at the oxygen evolving complex with spin markers under photoelectric polarization

Pei-Ying Huo,¹ Wei-Zhou Jiang,^{1,*} Rong-Yao Yang,¹ and Xiu-Rong Zhang²

¹*School of Physics, Southeast University, Nanjing 211189, China*

²*School of Science, Jiangsu University of Science and Technology, Zhenjiang 212100, China*

Water oxidation at the oxygen evolving complex (OEC) of the photosystem II is catalyzed by the core cluster CaMn_4O_5 which was projected to experience five intermediate states S_i in the Kok's cycle since 1970's. However, the detailed dynamics of state evolutions still remains unclear, albeit with the general fact that the process is initiated by the transfer of photoelectrons with the steady electron donors of the water molecules. Based on density functional simulations, we find that the spin flips of Manganese atoms between the consecutive states in the electric polarization field can be used as a marker to uncover the intricate dynamic evolutions and the underlying dynamics. The dynamic electron and proton transfers and water insertion and dissociation are traced to reveal the evolution pathways of S_0 - S_3 with commensurate spin flips towards the exact spin configuration of the next state. In particular, the various water insertions and dissociations at coordination sites of the S_2 open and closed cubane isomers are predicted with constraints on the necessary spin flips. Our study paves a way to uncover the animated OEC evolutions with the spin flips that await for more experimental verifications and lays a solid ground for revealing the mechanism of dioxygen generation via the pending S_4 state.

I. INTRODUCTION

In nature, the solar energy is converted into the biochemical energy in the photosynthetic process that enables the self-sustained biological circulation on the Earth [1]. In the cascade photosynthetic process, one of the most fundamental reactions is the water oxidation catalyzed at the oxygen evolving complex (OEC). Not only does the water oxidation release the molecular oxygen to refresh the atmosphere vitally in the industrial age, but provides the logistic supply of 4 electrons and 4 protons in a closed circle to convert carbon dioxide into the organic molecules. The catalytic pathway of the OEC is known as the Kok's cycle [2] that circulates through five redox states ($S_i, i = 0, \dots, 4$), driven by the carousel of photoelectron in the Photosystem II (PSII) reaction centre, P_{680} . In the past, great endeavor both in experiments and simulations has been made to identify the structures of OEC states $S_{i=0, \dots, 3}$ prior to the dioxygen generation at S_4 whose structure was reported most recently [3]. Since the mechanism of molecular oxygen formation still remains rather elusive, the standing effort to reveal the OEC structures and dynamic evolutions is important not only for understanding the nature of water oxidation but also for designing the catalysts to develop clean energy [4–6].

Since the OEC core structure in the dark stable state (S_1) was first revealed by high resolution X-ray diffraction in 2011 [7], experimental and computational efforts have further been made to achieve outstanding progresses such as refining respective S_i structures [1, 8–15], determining oxidation states [16–21], and spin orientations [16, 22–24] of Mn atoms. However, the evo-

lution pathway of the OEC states prior to the dioxygen generation, especially $S_2 \rightarrow S_3$ that involves water insertion, electron and proton transfers, still remains quite unclear in details. The S_2 state features two EPR signals with $g=2$ and 4.1 which were identified by computational studies to be the low-spin open and high-spin closed cubane isomers (S_{2-a} and S_{2-b}), respectively [10]. The evolution of $S_2 \rightarrow S_3$ may thus suggest several possible paths, with variations arising from the substrate water molecules (W2 or W3), the function of two isomers and the exact sequence of the three events [25–32], and the transition from S_{2-a} to S_{2-b} in the evolution path was once regarded as a key mechanism to obtain the high spin ($S=3$) of the S_3 state [23]. Recently, the insertion of water in the S_2 open cubane isomer in the evolution process has gained mounting support [25, 33–35]. It was reported that the protonation of O_4 in S_{2-a} can induce a low-spin to high-spin transition from $1/2$ to $5/2$ (or even $7/2$) without structural isomerization [36, 37]. Actually, the detail how the spin of various states evolves and the dynamics that dictates the spin flip remain unclear to large extent due to the complexity subject to the dynamic complex system. These issues are not limited to $S_2 \rightarrow S_3$ but pervasive in the evolution of the whole Kok's cycle.

The state evolution is triggered by the polarization effect of the positive-charged hole after the transfer of the photoproduced electron at P_{680} . The hole polarization field drives the electron transfer from the core Mn_4Ca that breaks the time reversal symmetry associated with the spin flips of the state. The spin flips can thus reflect an irreversible time sequence of the evolution. More importantly, the spin flip can serve as a significant indicator to reveal the detail of the dynamic evolution, because it is associated tightly with the variation of the polarization field and the resultant charge transfers. In fact, the electric polarization provides a gradient field that modifies

* Corresponding author: wzjiang@seu.edu.cn

the Coulomb potential, while the change in the Coulomb potential can shift the spin or orbital motion, in that the spin-orbit coupling potential is determined by the gradient of the Coulomb potential according to the Dirac equation of charged particles. In addition, the bonding electrons in molecular orbitals, restricted by the Pauli exclusion principle, are characterized by their spin states in the Coulomb potential. Thus, the electric polarization should naturally result in the shift of the spin dynamics of atoms in the OEC. In this work, we study for the first time the polarization effect on the OEC cycle. In particular, with the density functional simulations, we explore the spin flips of Manganese atoms and reveal the dynamic mechanisms of state evolutions of S_0 - S_3 , driven by the polarization of the photoelectric hole at P_{680} .

II. COMPUTATIONAL METHODS

We perform the spin-polarized all-electron density functional simulations with the DMol³ package in the Materials Studio of Accelrys Inc. The OEC system in the simulation is intercepted from the XRD crystal data obtained at 1.9 Å resolution by Yasufumi Umena[7] from protein data bank (PDB ID: 3WU2). As shown in the Fig. 1a, the selected configuration is composed of the core structure (CaMn_4O_5) and its nine surrounding amino acids (His332, Glu189, Asp342, Ala344, Asp170, Glu333, CP43-Glu354, His337, CP43-Arg357), as well as eight water molecules. Eventually, the system contains 112 atoms. In the geometric optimization process, we adopt the Perdew-Burke-Ernzerhof (pbe) exchange correlation functional within the general gradient approximation (GGA) and the double numerical basis set plus polarization (DNP). Optimization accuracy of the energy is set to be 2.0×10^{-5} Hartree. All eight possible Mn spin configurations of CaMn_4O_5 structure are considered during the optimization procedure and the lowest energies are regarded as the S_i structures. Mn oxidation states are calculated by both the Mulliken spin populations and the bond valence sum (BVS). In the BVS calculation, relevant parameters are taken from the Ref. [38].

The hole polarization effect following each light-driven electron separation at P_{680} is simulated by putting an effective point charge (denoted as Q_h) at the tyrosine residue (Tyr161). Electron separation at P_{680} leads to oxidation of Tyr161, which subsequently oxidizes the core CaMn_4O_5 . Note that some computational calculations and experiments suggested that the Tyr161 oxidation is followed by a reciprocal deprotonation toward His190 and leaves a neutral radical [39–41]. The proton migrates back to Tyr161 with a cooperative electron transfer from the CaMn_4O_5 . This is actually a rather complicated process, while we make a simple comparison to the case with a positive point charge put at His190. It is found that the resulting spin flips and system energies are consistent for the electron transfer. Additionally, simulations confirm the negligible difference in the impact of the spe-

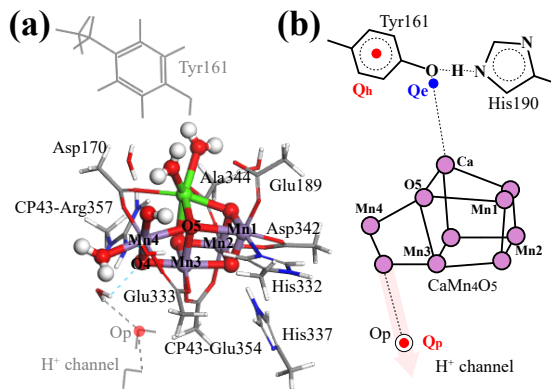


FIG. 1. (a) Geometric model of the OEC CaMn_4O_5 , along with surrounding ligated amino acid residues. Purple, green, red, grey, blue and white spheres represent Mn, Ca, O, C, N, H atoms, respectively. The Tyr161 outside of the OEC and one proton transfer channel, denoted by O_p , are also sketched. (b) Schematic diagram for the positions of effective point charges set in the simulation. The red and blue solid circles represent positive and negative point charges, respectively.

cific location of the hole at the central or peripheral C or O atoms of Tyr161. Based on these verifications, we eventually place Q_h at the central site of Tyr161. Considering the distance and screening effects, the effective charges of $Q_h \approx 0.1e$ and $Q_h=1.0e$ at the Tyr161 correspond to the photoelectric hole generation at P_{680} and Tyr161 oxidation, respectively. Intrigued by the hole polarization effect, the electron and proton are deprived sequentially from the core CaMn_4O_5 cluster. During deprivations of electrons and protons along e^-/H^+ transfer channels, the polarization effect is also produced by the moving electrons (Q_e) and protons (Q_p). The polarization effects by both the hole and moving electron and proton are simulated by putting the equivalent point charges at some typical places under the constraint of the charge conservation of the whole system to track the dynamic process of state evolution. The point charge for simulating the moving electron (Q_e) is placed close to Tyr161 and typically at a distance of 4 Å away from Ca atom of CaMn_4O_5 on the line connecting to the O atom of Tyr161, see Fig. 1b. The specific choice of the charge site is partly associated with the fact that the proton migrations with a cooperative electron transfer take place near the O atom after the Tyr161 oxidation. Meanwhile, it is verified that varying Q_e 's location on the various lines pointing towards the O, C atoms and centre of Tyr161 at a distance of 4 Å away from the Ca atom of CaMn_4O_5 does not change the main results concerning the spin flips of Mn atoms. The polarization effect of the moving proton is simulated by putting the equivalent point charge of 1.0e at the site O_p near the O atom along the H^+ transfer channel, as shown in Fig. 1.

III. RESULTS AND DISCUSSION

A. Structures of S_0 - S_3 states

In recent years, there has been a noteworthy progress in revealing the structural details of the states $S_i, i = 0, \dots, 3$. The $Mn_1 \sim Mn_4$ oxidation states for S_0 - S_3 states are suggested by experimental and computational studies to be in turn (III, IV, III, III) \rightarrow (III, IV, IV, III) \rightarrow (III, IV, IV, IV)/(IV, IV, IV, III) \rightarrow (IV, IV, IV, IV) for $S_0 \rightarrow S_1 \rightarrow S_{2-a}/S_{2-b} \rightarrow S_3$ [8, 16, 42]. Various measurements by the extended x-ray absorption fine structure (EXAFS) have revealed a consistent picture of the Mn-Mn distances of each S state [16]. The spin configurations of Mn atoms in S_0 - S_3 states are also identified: $\uparrow\downarrow\uparrow\downarrow$ in the S_0 state in which one proton is assigned to the O_5 [23], $\uparrow\downarrow\downarrow\uparrow$ in the dark-stable state S_1 with the ground state spin $S_{GS}=0$ [43, 44], $\uparrow\downarrow\downarrow\uparrow$ and $\uparrow\uparrow\downarrow\uparrow$ for two S_2 isomers S_{2-a} and S_{2-b} , respectively [22, 23], and $\uparrow\uparrow\downarrow\uparrow$ or $\uparrow\uparrow\downarrow\uparrow$ for S_{3-a} and $\uparrow\uparrow\downarrow\uparrow$ for S_{3-b} [16, 23]. Note that there are some uncertainties in S_3 structure arising from three measurements by the X-ray free electron laser (XFEL) during 2016-2018 [11–13]. It was reported in 2016 that no additional water or hydroxo bond to the OEC was observed in S_3 [11], whereas other two measurements confirmed the presence of an additional oxygen ligand but with different O_5 - O_6 (O_x) distances [12, 13]. The simulations show there exist two S_3 isomers, S_{3-a} and S_{3-b} , obtained from S_{2-a} and S_{2-b} by adding one hydroxyl, respectively [30, 45]. Our optimized structures for S_0 - S_3 including the Mn-Mn bond distances, oxidation states and spin configurations of Mn atoms are displayed in Fig. 2, which are consistent with those in the literature mentioned above.

B. Dynamic evolutions of S states

Prior to the analysis of the specific dynamic evolution, it is necessary to understand the force with the underlying potential that drives the evolution of S states. The OEC cycle starts with the production of the photoelectric hole after the photoelectron separation, which exerts an electric polarization effect on Tyr161 and OEC. The presence of the polarization effect naturally adds the modification to the Coulomb field gradient appearing in the second-order Dirac equation of charged particles. The gradient term is given as

$$\xi(r) = -\frac{1}{2m_e^2 c^2} \vec{\sigma} \cdot (\hat{\mathbf{p}} \times \nabla V), \quad (1)$$

where V is the Coulomb potential and $\vec{\sigma}$ the spin Pauli matrices. In the central force, Eq.(1) just represents the spin-orbit coupling term: $\xi(r) = \vec{\sigma} \cdot \hat{\mathbf{L}} / (2m_e^2 r c^2) dV/dr$, with the angular momentum operator $\hat{\mathbf{L}}$ obtained from the curl calculation. In the specific density functional, the contribution of $\xi(r)$ should be included appropri-

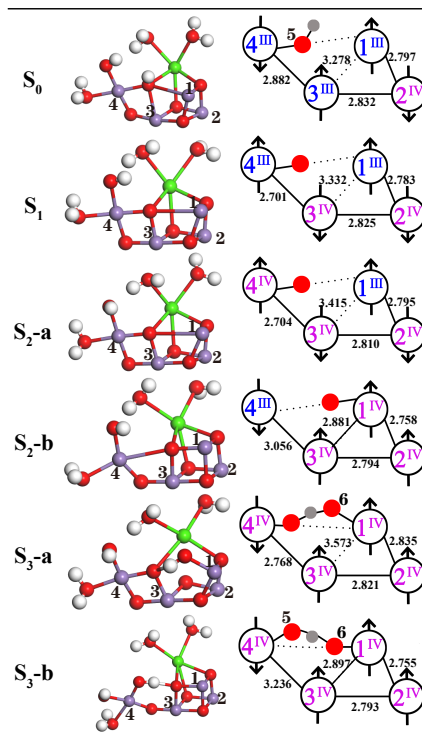


FIG. 2. Optimized structures of the S_0 - S_3 states. Shown on the right column are Mn-Mn distances (Å), spin orientations and oxidation states of Mn atoms.

ately in the potential terms of the Kohn-Sham equations. The modification of the Coulomb field gradient can thus shift the spin orientations of unpaired electrons and affect the electron orbitals. The spin states of atoms, restricted by the Pauli exclusion principle, are informative for the bonding properties and orbital motions of the molecule due to the spin-orbit interaction. Also, the electron spins on the hybrid orbitals can also reflect the structural properties including electron spatial configuration of molecules. While different spin states of atoms correspond definitely to different quantum states and valence bond properties, the spin flips under the polarization field of the positive-charged hole and moving electrons and protons can be used as a marker to track the dynamic evolution of the S state, providing a theoretical criterion to determine the controversial evolution pathways.

As the potential in the density functional equations is modified by the polarization field, the obtained electron wave functions and density distributions undergo the change accordingly. Here we present an example of the electron distribution variations of the S_1 state in the polarization field produced by the electron hole at the Tyr161 and the electron transfer. Shown in Fig. 3 are the sectional electron density distributions of the S_1 state in various cases. We can observe some significant variations in the electron density distributions and geometric structures arising from the various polarization effects. When the hole polarization is imposed on the S_1 state,

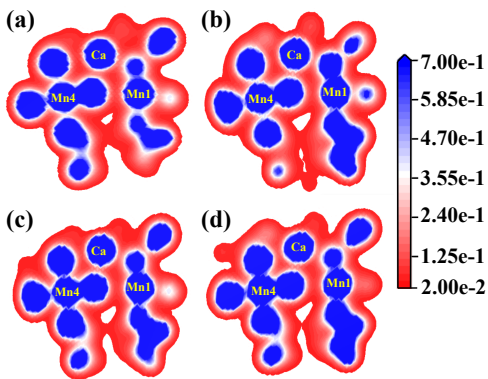


FIG. 3. Sectional profiles of the electron density distributions at the Ca-Mn₁-Mn₄ plane

. Slices (a), (b), (c) and (d) stand for the cases for the pure S₁ state, with the hole at the Tyr161, with the transferring effective charge Q_e of $-0.5e$ and $-0.9e$ 4 Å away from the Ca atom of CaMn₄O₅, respectively.

the striking changes in the density profiles can be observed, as compared with the right and lower regions of Fig. 3a,b. On the lower part of Fig. 3a,b, the relative change arises mainly from the tilting and prostrating of the amino acid residues induced by the polarization field. As the charge of the moving electron increases, the significant changes also occur at edge parts including the amino acid residues, see the relative changes in Fig. 3a,b,c. As these variations are induced by the underlying changes in the Coulomb potential that are associated with the spin-space (orbit) coupling, as seen in Eq.(1), using the spin as a marker can point to the intermediate state structures that are characterized by the spin of atoms, electron density distributions and geometric features consistently in the dynamic evolution intrigued by the polarization field.

S₀ → S₁. The hole polarization field at P₆₈₀ leads to oxidation of Tyr161 and subsequently the CaMn₄O₅. At first, we employ a simple model without Tyr161 oxidation to simulate the hole polarization field which is numerically realized by placing an equivalent positive charge of 0.1e at the Tyr161 considering the screening effect at a long distance. On the way of the electron transfer towards the hole at P₆₈₀, the effective charge of the hole reduces for the charge neutralization, and this is simulated by reducing the equivalent charge at the Tyr161 under the constraint of the charge conservation of the whole system. After the simulation of this simple model, we consider the more realistic process of Tyr161 oxidation that occurs in a time scale of the nanoseconds to microseconds and the CaMn₄O₅ oxidation in the time scale of the microseconds to milliseconds [41, 46–49]. After the oxidation of Tyr161 and the subsequent charge annihilation at the P₆₈₀, the hole polarization field at the Tyr161 dominates the oxidation of the CaMn₄O₅. In this case, the positive charge of $Q_h=e$ is placed at the Tyr161 to simulate the dynamic oxidation process and the evolution from the S₀ to S₁. We mimic the pathway

of the electron transfer from the CaMn₄O₅ to the Tyr161 dynamically by guaranteeing correct spin flips of the Mn atoms from the S₀ to S₁.

The presence of the hole polarization with the equivalent Q_h of 0.1e point charge at the Tyr161 causes the Mn₄ spin of S₀ state flips surely due to the change of the gradient of the Coulomb field. And the total energy increases under the hole polarization field, suggesting the higher structural activity that is more suitable for the state evolution. Driven by the hole polarization, one electron and subsequently one proton start to be deprived from the CaMn₄O₅ for the evolution S₀→S₁ [50]. In a simulation that the moving electron approaches the hole with the gradual Q_h decrease starting from 0.1e, the Mn spin configuration remains $\uparrow\downarrow\uparrow\downarrow$, whereas the Mn₃-O₅ distance gradually decreases to 1.975 Å. Since the Mn oxidation state depends on the proximity with the surrounding O atoms, the shortening of Mn₃-O₅ distance accounts for the transition of the oxidation state of Mn₃ to IV, which is supported by both Mulliken population and BVS calculations. Subsequently, the proton assigned to the O₅ is transferred, and the Mn spin configuration changes to $\uparrow\downarrow\uparrow\uparrow$, which is exactly in accordance with the spin of S₁ state.

Besides the simulation in a simple model, we investigate the evolution that is driven by the oxidation of the positive-charged hole at the Tyr161. The simulation with the hole polarization field, induced by Tyr161 oxidation, also successfully reveals the spin flips of the Mn atoms in processes of the electron and proton deprivation and transfer. The Mn spin configuration changes from $\uparrow\downarrow\uparrow\downarrow$ to $\uparrow\downarrow\uparrow\uparrow$ under the hole polarization field. Owing to the close relationship between the spins and valence bond properties, the spin flips of the key atoms means the structural change of the molecule that puts the OEC state on a track of the dynamic evolution. It is found that the distances of some key bonds undergo significant changes in the hole polarization field. For instance, we notice that the Mn₃-O₅ distance elongates from 2.263 Å to 2.344 Å, compared to the slight changes (<0.02 Å) in other Mn-O distances, which implies the weakening of the coupling strength between Mn₃ and O₅. As the coupling is specified by the equivalent charge of the bonding atoms, the changes in the equivalent charge and bonding distances can play a role of the precursor in the electron transfer in the dynamic evolution. To mimic the dynamic process of the electron transfer gradually towards the Tyr161 hole, we put an effective charge Q_e changing from $-0.1e$ to $-0.9e$ at the position 4 Å away from the Ca atom of CaMn₄O₅ on the line connecting to the O atom of Tyr161 shown in Fig. 1b. Consequently, the polarization effect, produced by the hole ($Q_h=e$) and moving electron, diminishes and eventually vanishes when the moving electron fully recombines with the hole. In this process, along with the Mn₃-O₅ distance decreasing, the Mn spin configuration goes through $\uparrow\downarrow\uparrow\downarrow$ and $\uparrow\downarrow\uparrow\uparrow$ and back to $\uparrow\downarrow\uparrow\downarrow$ again, as shown in the blue dashed line box between the states

S_0 and S_1 in Fig. 4. Then, the Mn spin configuration transits to that of the S_1 state after the proton removal.

In both cases, we see that the polarization effect of the hole directly causes the change of the bond lengths, the spin flips of Mn atoms, and the OEC oxidation with the charge transfer. Using the spin flip as a marker to points to the pathway of the moving electron and proton, we successfully illustrate the dynamic evolution of the state S_0 to S_1 , which also provides a paradigm for exploring the subsequent state evolutions by watching the spin flips of the Mn atoms.

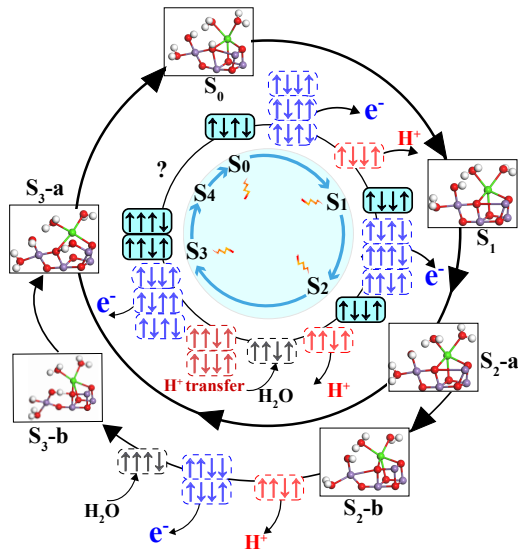


FIG. 4. Schematic diagram of the S_i state cycle with the spin markers. The blue and red dashed boxes show the transient Mn spin configurations during electron and proton transfer under the hole polarization.

$S_1 \rightarrow S_2$. A key object in understanding the $S_1 \rightarrow S_2$ that involves only one electron transfer is to identify the terminal state in the presence of the two S_2 isomers. In the simple model with the effective charge Q_h of 0.1e placed at the central site of Tyr161, the Mn spin configuration changes through $\uparrow\downarrow\uparrow\downarrow$ to $\uparrow\downarrow\uparrow\uparrow$ during the electron transfer process as Q_h gradually decreases from 0.1e. On the other hand, the realistic hole polarization field produced by Tyr161 oxidation causes the Mn spin configuration to transit eventually to $\uparrow\downarrow\uparrow\uparrow$ through the intermediate states $\uparrow\downarrow\uparrow\downarrow$, $\uparrow\uparrow\uparrow\downarrow$ and $\uparrow\uparrow\downarrow\uparrow$, as the moving electron approaches the hole, as shown in the blue dashed boxes between the states S_1 and S_2 in Fig. 4. In both cases, the evolution of $S_1 \rightarrow S_2$ reaches the ultimate Mn spin configuration of $\uparrow\downarrow\uparrow\uparrow$, which designates the open-structure of S_2 , the S_2 -a isomer. During the evolution process, we observe that the Mn_1 - O_5 distance increases generally, which also supports that S_2 -a is the terminal state of the S_1 evolution. Here, we stress that the spin marker identifies the terminal state S_2 -a of the evolution, while the S_2 -b can be converted from S_2 -a as two isomers are interconvertible [10, 26].

$S_2 \rightarrow S_3$. The $S_2 \rightarrow S_3$ transition is a rather complex process that involves the insertion of water and the transfer of an electron and a proton. The exact sequence of these three events is not very clear yet, although various experimental measurements have confirmed that the proton removal takes place before the electron transfer [33, 50–54]. Besides, it remains an hot issue to identify the pathway of the substrate water insertion and the specific roles of two S_2 isomers in the evolution process.

In the simulations, we consider all possible substrate water insertions, sequences of the electron and proton transfers, and the participation of the two isomers. Using the spin flip between the initial and terminal states as a marker, we can determine the candidate pathways of the evolution by ruling out others that are not compatible with the necessary spin flips. With the correct spin flips of Mn atoms, dynamic evolution paths with and without transitions between open and closed cubane isomers are denoted as path-1 and path-2, respectively, as shown in Fig. 5.

The path-1 starts from the S_2 -a isomerization to S_2 -b and then follows the sequence of the proton and electron transfers and water insertion. The proton transfer of W1 gives rise to structural rearrangement and opens an accessible coordination site for the cascade water insertions. As a result, the hydroxyl (W2) is inserted between Mn_4 and O_5 in the intermediate state denoted as S_2 -b' in Fig. 5. At this moment, the Mn spin configuration changes to $\uparrow\uparrow\uparrow\downarrow$ as displayed in the simulations for both cases of the simple model and of the realistic hole at the Tyr161. The subsequent electron transfer makes the Mn spin configuration change to $\uparrow\uparrow\uparrow\downarrow$. In a dynamic simulation through increasing the effective charge of the transferring electron Q_e , we can observe that the Mn spin configuration undergoes $\uparrow\uparrow\downarrow\downarrow$ and $\uparrow\downarrow\downarrow\uparrow$ till to $\uparrow\uparrow\uparrow\downarrow$, which reveals a dynamic process of the transient spin evolution. Once the electron transferred from the OEC recombines with the hole, the polarization field vanishes until the hole is regenerated in the next photoelectric process at P₆₈₀. Note that the principal spin flip from the low-spin S_2 to high-spin S_3 in path-1 is realized at the transition from the state S_2 -a to S_2 -b, similar to that in Refs. [23, 26, 30]. Then, the water insertion can take place spontaneously. The experimental ammonia binding result and computational calculations claimed that a water molecule W_x around O_4 , approaching close to Mn_4 , causes the W1 and W2 to be displaced, see the diagram (E) of Path-1 in Fig. 5 [29–32, 55]. In our simulations, it shows that the energy of the system decreases by 0.256 eV after the water insertion, which indicates that W_x as a substrate water is energetically favored.

The water insertion into the S_2 open cubane has gained substantial support most recently [25, 33, 35, 56]. In our simulations, this is subject to the path-2 free of a transition to S_2 -b closed cubane isomer. The path-2 starts with the proton removal from W1 under the hole polarization field, resulting in the Mn spin configuration change to $\uparrow\uparrow\uparrow\uparrow$ in the simulation for both simple model

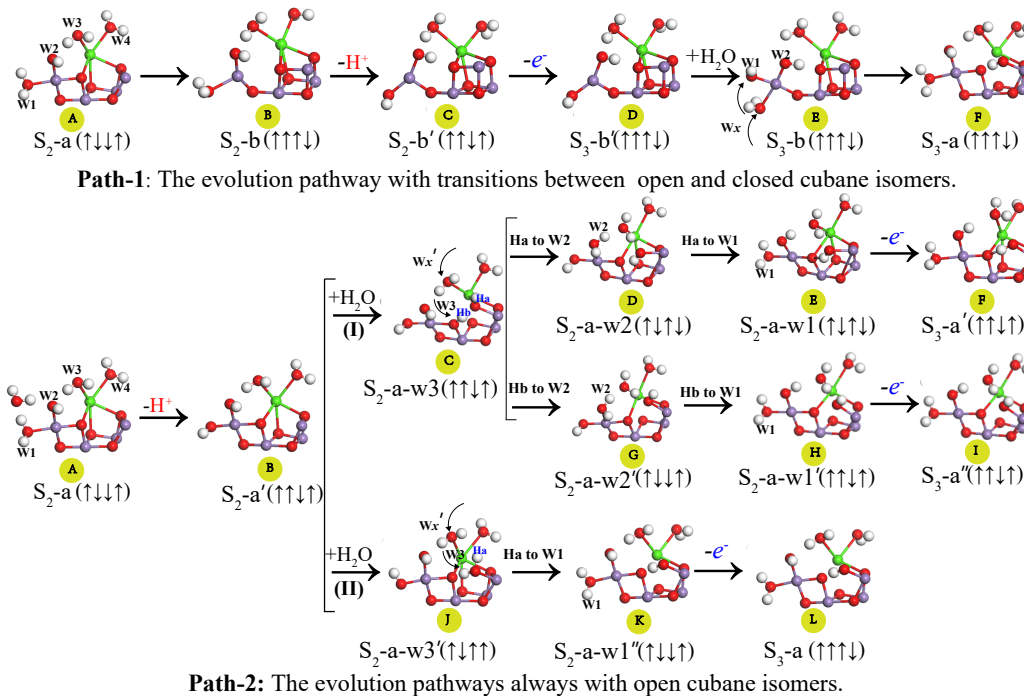


FIG. 5. Evolution pathways for $S_2 \rightarrow S_3$ with and without transitions between the open and closed cubane isomers, denoted as path-1 and path-2, respectively. The evolution includes the proton ($-H^+$) and electron ($-e^-$) transfers and the water insertion ($+H_2O$) as marked, and the states after the electron transfer are dubbed S_3 states. W_x or W_x' represents the ambient water on the insertion pathway. In path-2, branches (I) and (II) represent two different W_3 insertion, and in path-2 (I), two H^+ from W_3 in the diagram (C) are marked as Ha and Hb, respectively.

and the realistic hole at Ty161. Subsequently, W_3 is inserted as a substrate water between Mn_1 and O_5 . During the $S_2 \rightarrow S_3$, it is noteworthy to show that the amino acid Glu189 moves away from Ca and Mn_1 - Mn_4 distance elongates, as also reported in Ref. [33] with the observation around $50 \sim 150 \mu s$. These structural changes are closely related to the event of the W_3 insertion. With some path dependence of the insertion, the W_3 can be inserted in two forms: either as a spontaneous dissociation of OH^- and H^+ or as the H_2O , as shown on the branch (I) and (II) of path-2 in Fig. 5 where the intermediate states are denoted by S_{2-a-w3} on path-2 (I) and $S_{2-a-w3'}$ on path-2 (II), respectively. Along the path-2 (I) from the diagram (C), one of protons from W_3 , denoted as Ha or Hb, transfers through W_2 to W_1 . With the Ha transfer by option, the spin configuration of Mn changes to $\uparrow\downarrow\downarrow$, corresponding to the path from diagram (D) to (E) of path-2 (I) in Fig. 5. In the case of the Hb transfer, the Mn spin configuration changes through $\uparrow\downarrow\downarrow$ to $\uparrow\downarrow\uparrow$, which is the path from the diagram (G) and (H) of path-2 (I). In the subsequent simulations, as the moving electron approaches the hole, the Mn spin configuration goes through $\uparrow\downarrow\downarrow$, $\uparrow\downarrow\uparrow$ and $\uparrow\downarrow\downarrow$ to $\uparrow\downarrow\downarrow$ in the path to diagram (F) and undergoes $\uparrow\downarrow\downarrow$ to $\uparrow\downarrow\downarrow$ in the path to diagram (I). Here, the $\uparrow\downarrow\downarrow$ of $S_{3-a'}$ in the diagram (I) is a Mn spin configuration confirmed by the ^{55}Mn hyperfine coupling constants in the S_3 state [16, 17]. Besides this path with the Hb removal, in our simulation

another isomer is predicted with the same spin configuration induced by the Ha removal. Along the path-2 (II) with the intact H_2O insertion at the state $S_{2-a-w3'}$, the proton Ha then transfers to W_1 . At this step, the constraint calculations are performed to obtain the Mn spin configuration of the low-lying state amongst all possible intermediate states. It is the intermediate state $S_{2-a-w1''}$ with the spin configuration $\uparrow\downarrow\downarrow$ that evolves to an energetically favorable state with the spin configuration $\uparrow\uparrow\downarrow$, next to the subsequent electron transfer. Note that this Mn spin configuration of the state S_{3-a} in the diagram (L) is consistent with that reported spin of S_3 in Refs [16, 23].

It is necessary to mention that the final-state geometric and electronic structure together with its spin configuration in path-2 is rather dependent on the intermediate state prior to the electron transfer. This dependence is largely ascribed to a rather flat potential energy surface of the intermediate states in a multi-step evolution to the S_3 state. In addition, the multiple spin flips between the low and high spin configurations in path-2 may imply that the spin exchange interaction plays an active part in the present functional and thus a comprehensive consideration of the exchange interaction seems to be necessary in more accurate functionals. Though recent experiments have made remarkable achievements in discriminating the main evolution stages [25, 33, 35, 56], our predictions that reveal the extensive details and in-

formation of the dynamic evolution, especially those belonging to the intermediate states, remain to be verified by experiments in the future.

In this work, we are mainly dedicated to the specification and characterization of the polarization effect on the OEC evolution with a medium-size model that does not include the Tyr161 in the density functional simulations. Some dynamic aspect associated with the Tyr161 structure may thus be missing. For instance, the switch effect of the hydrogen bond connecting the O atom of Tyr161, which is predicted in the Tyr161 oxidation [39], is absent in the simulations. While we performed the simulations of the polarization effect by putting an equivalent positive point charge at Tyr161, the subsequent impact of tyr161 oxidation is actually included phenomenologically on the water orientation and the OEC system. Yet, expanding our model would be necessary to include more dynamic content in future.

IV. SUMMARY

We have investigated the static properties and the dynamic evolution of the oxygen evolving complex from the state S_0 to S_3 driven by the polarization field of the photo-produced hole using the density functional method. The simulation with appropriate modelling of the polarization field shows that the Mn spin flips occur with relevant structural changes in key Mn-O distances which can serve as the precursor of losing electron from relevant Mn atoms. Constrained by the geometric and electronic

structure of various states, the emphasis was put on the dynamic evolution traced by the spin marker that points to the correct spin configuration of the next state. In the processes of $S_0 \rightarrow S_2$, the corresponding spin flips, following the electron and proton transfers, are displayed dynamically under the evolving polarization field. For the multi-step evolution of $S_2 \rightarrow S_3$ with water insertion, we reconstructed the evolution pathways, consistent with the main intermediate stages captured by the observations. In particular, a spontaneous water dissociation between Mn_4 and O_5 was observed with the new finding of the two final-state isomers with the same spin configuration. Our study paves a way to uncover the animated evolutions of the Kok's cycle with spin flips and lays a solid ground for revealing the mechanism of dioxygen generation by reestablishing the elusive S_4 state guided by the spin flips.

ACKNOWLEDGEMENT

We thank Profs. Xi-Jun Qiu, Han-Sen Gu and Dr. Shi-Jun Yuan for some early instructive discussions. This work was supported in part by the National Natural Science Foundation of China under grants No. 11775049 and No. 12375112 and the China Postdoctoral Science Foundation under grant No. 2021M690627. The Big Data Computing Center of Southeast University is acknowledged for providing the facility support on the partial numerical calculations of this work.

-
- [1] J.-R. Shen, *Annual review of plant biology* **66**, 23 (2015).
 [2] B. Kok, B. Forbush, and M. McGloin, *Photochemistry and Photobiology* **11**, 457 (1970).
 [3] P. Greife, M. Schönborn, M. Capone, R. Assunção, D. Narzi, L. Guidoni, and H. Dau, *Nature*, 1 (2023).
 [4] C. Zhang, C. Chen, H. Dong, J.-R. Shen, H. Dau, and J. Zhao, *Science* **348**, 690 (2015).
 [5] B. Zhang and L. Sun, *Dalton Transactions* **47**, 14381 (2018).
 [6] A. J. Wilson and P. K. Jain, *Journal of the American Chemical Society* **140**, 5853 (2018).
 [7] Y. Umena, K. Kawakami, J.-R. Shen, and N. Kamiya, *Nature* **473**, 55 (2011).
 [8] M. Suga, F. Akita, K. Hirata, G. Ueno, H. Murakami, Y. Nakajima, T. Shimizu, K. Yamashita, M. Yamamoto, H. Ago, *et al.*, *Nature* **517**, 99 (2015).
 [9] M. Askerka, D. J. Vinyard, J. Wang, G. W. Brudvig, and V. S. Batista, *Biochemistry* **54**, 1713 (2015).
 [10] D. A. Pantazis, W. Ames, N. Cox, *et al.*, *Angewandte Chemie International Edition* **51**, 9935 (2012).
 [11] I. D. Young, M. Ibrahim, R. Chatterjee, S. Gul, F. D. Fuller, S. Koroidov, A. S. Brewster, R. Tran, R. Alonso-Mori, T. Kroll, *et al.*, *Nature* **540**, 453 (2016).
 [12] M. Suga, F. Akita, M. Sugahara, M. Kubo, Y. Nakajima, T. Nakane, K. Yamashita, Y. Umena, M. Nakabayashi, T. Yamane, *et al.*, *Nature* **543**, 131 (2017).
 [13] J. Kern, R. Chatterjee, I. D. Young, F. D. Fuller, L. Lassalle, M. Ibrahim, S. Gul, T. Fransson, A. S. Brewster, R. Alonso-Mori, *et al.*, *Nature* **563**, 421 (2018).
 [14] R. Pal, C. F. Negre, L. Vogt, R. Pokhrel, M. Z. Ertem, G. W. Brudvig, and V. S. Batista, *Biochemistry* **52**, 7703 (2013).
 [15] X. Li, P. E. Siegbahn, and U. Ryde, *Proceedings of the National Academy of Sciences* **112**, 3979 (2015).
 [16] V. Krewald, M. Retegan, N. Cox, J. Messinger, W. Lubitz, S. DeBeer, F. Neese, and D. A. Pantazis, *Chemical Science* **6**, 1676 (2015).
 [17] N. Cox, M. Retegan, F. Neese, D. A. Pantazis, A. Bous-sac, and W. Lubitz, *Science* **345**, 804 (2014).
 [18] S. Petrie, R. J. Pace, and R. Stranger, *Angewandte Chemie* **127**, 7226 (2015).
 [19] R. Terrett, S. Petrie, R. Stranger, and R. J. Pace, *Journal of inorganic biochemistry* **162**, 178 (2016).
 [20] B. Baituti, *Journal of Theoretical and Computational Chemistry* **17**, 1850007 (2018).
 [21] N. Schuth, I. Zaharieva, P. Chernev, G. Berggren, M. Anderlund, S. Styring, H. Dau, and M. Haumann, *Inorganic chemistry* **57**, 10424 (2018).
 [22] D. Bovi, D. Narzi, and L. Guidoni, *New Journal of Physics* **16**, 015020 (2014).

- [23] V. Krewald, M. Retegan, F. Neese, W. Lubitz, D. A. Pantazis, and N. Cox, *Inorganic chemistry* **55**, 488 (2016).
- [24] R. Chatterjee, G. Han, J. Kern, S. Gul, F. D. Fuller, A. Garachtchenko, I. D. Young, T.-C. Weng, D. Nordlund, R. Alonso-Mori, *et al.*, *Chemical science* **7**, 5236 (2016).
- [25] F. Allgöwer, A. P. Gamiz-Hernandez, A. W. Rutherford, and V. R. Kaila, *Journal of the American Chemical Society* **144**, 7171 (2022).
- [26] D. Bovi, D. Narzi, and L. Guidoni, *Angewandte Chemie* **125**, 11960 (2013).
- [27] M. Shoji, H. Isobe, and K. Yamaguchi, *Chemical Physics Letters* **636**, 172 (2015).
- [28] I. Ugur, A. W. Rutherford, and V. R. Kaila, *Biochimica et Biophysica Acta (BBA)-Bioenergetics* **1857**, 740 (2016).
- [29] M. Askerka, D. J. Vinyard, G. W. Brudvig, and V. S. Batista, *Biochemistry* **54**, 5783 (2015).
- [30] M. Retegan, V. Krewald, F. Mamedov, F. Neese, W. Lubitz, N. Cox, and D. A. Pantazis, *Chemical Science* **7**, 72 (2016).
- [31] M. Capone, D. Bovi, D. Narzi, and L. Guidoni, *Biochemistry* **54**, 6439 (2015).
- [32] M. Capone, D. Narzi, D. Bovi, and L. Guidoni, *The journal of physical chemistry letters* **7**, 592 (2016).
- [33] M. Ibrahim, T. Fransson, R. Chatterjee, M. H. Cheah, R. Hussein, L. Lassalle, K. D. Sutherlin, I. D. Young, F. D. Fuller, S. Gul, *et al.*, *Proceedings of the National Academy of Sciences* **117**, 12624 (2020).
- [34] P. E. Siegbahn, *Physical Chemistry Chemical Physics* **20**, 22926 (2018).
- [35] R. Hussein, M. Ibrahim, A. Bhowmick, P. S. Simon, R. Chatterjee, L. Lassalle, M. Doyle, I. Bogacz, I.-S. Kim, M. H. Cheah, *et al.*, *Nature communications* **12**, 6531 (2021).
- [36] T. A. Corry and P. J. O' Malley, *The Journal of Physical Chemistry Letters* **10**, 5226 (2019).
- [37] T. A. Corry and P. J. O' Malley, *Journal of the American Chemical Society* **142**, 10240 (2020).
- [38] W. Liu and H. H. Thorp, *Inorganic Chemistry* **32**, 4102 (1993).
- [39] S. Nakamura, M. Capone, D. Narzi, and L. Guidoni, *Physical Chemistry Chemical Physics* **22**, 273 (2020).
- [40] S. Nakamura, R. Nagao, R. Takahashi, and T. Noguchi, *Biochemistry* **53**, 3131 (2014).
- [41] S. Styring, J. Sjöholm, and F. Mamedov, *Biochimica et Biophysica Acta (BBA)-Bioenergetics* **1817**, 76 (2012).
- [42] V. K. Yachandra, V. J. DeRose, M. J. Latimer, I. Mukerji, K. Sauer, and M. P. Klein, *Science* **260**, 675 (1993).
- [43] D. Koulouglotis, D. J. Hirsh, and G. W. Brudvig, *Journal of the American Chemical Society* **114**, 8322 (1992).
- [44] T. Yamauchi, H. Mino, T. Matsukawa, A. Kawamori, and T.-a. Ono, *Biochemistry* **36**, 7520 (1997).
- [45] D. A. Pantazis, *Inorganics* **7**, 55 (2019).
- [46] K. Brettel, E. Schlodder, and H. Witt, *Biochimica et Biophysica Acta (BBA)-Bioenergetics* **766**, 403 (1984).
- [47] G. Christen, F. Reifarth, and G. Renger, *FEBS letters* **429**, 49 (1998).
- [48] F. Rappaport, M. Blanchard-Desce, and J. Lavergne, *Biochimica et Biophysica Acta (BBA)-Bioenergetics* **1184**, 178 (1994).
- [49] M. Haumann, P. Liebisch, C. Muller, M. Barra, M. Grabolle, and H. Dau, *Science* **310**, 1019 (2005).
- [50] A. Klauss, M. Haumann, and H. Dau, *Proceedings of the National Academy of Sciences* **109**, 16035 (2012).
- [51] S. M. Mäusle, A. Abzaliyeva, P. Greife, P. S. Simon, R. Perez, Y. Zilliges, and H. Dau, *The Journal of Chemical Physics* **153**, 215101 (2020).
- [52] I. Zaharieva, P. Chernev, G. Berggren, M. Anderlund, S. Styring, H. Dau, and M. Haumann, *Biochemistry* **55**, 4197 (2016).
- [53] H. Takemoto, M. Sugiura, and T. Noguchi, *Biochemistry* **58**, 4276 (2019).
- [54] H. Sakamoto, T. Shimizu, R. Nagao, and T. Noguchi, *Journal of the American Chemical Society* **139**, 2022 (2017).
- [55] J. Wang, M. Askerka, G. W. Brudvig, and V. S. Batista, *ACS energy letters* **2**, 2299 (2017).
- [56] Y. Okamoto, Y. Shimada, R. Nagao, and T. Noguchi, *The Journal of Physical Chemistry B* **125**, 6864 (2021).